IOPscience iopscience.iop.org

Home Search Collections Journals About Contact us My IOPscience

The lattice dynamics of the fluoroperovskite $KMgF_3$

This article has been downloaded from IOPscience. Please scroll down to see the full text article.

1993 J. Phys.: Condens. Matter 5 7615

(http://iopscience.iop.org/0953-8984/5/41/009)

View the table of contents for this issue, or go to the journal homepage for more

Download details:
IP Address: 171.66.16.96
The article was downloaded on 11/05/2010 at 02:00

Please note that terms and conditions apply.

J. Phys.: Condens. Matter 5 (1993) 7615–7622. Printed in the UK

The lattice dynamics of the fluoroperovskite $KMgF_3$

S Salaün†, M Mortier†, J Y Gesland†, M Rousseau† and B Hennion‡

† Equipe de Physique de L'Etat Condensé, URA CNRS No 807, Faculté des Sciences, 72017 Le Mans Cédex, France

‡ Laboratoire Léon Brillouin, CEN-Saclay, 91170 Gif-sur-Yvette Cédex, France

Received 21 May 1993, in final form 19 July 1993

Abstract. The low-frequency (< 9 THz) phonon dispersion curves in the main symmetry directions of the fluoroperovskite crystal $KMgF_3$ have been measured at room temperature by means of coherent inelastic neutron scattering. These dispersion curves are well described by a rigid-ion model. The mean square displacements (MSDs) of the ions and the phonon density of states are deduced.

1. Introduction

Many studies have been performed on fluoride compounds crystallizing with the perovskite structure, particularly on those presenting a solid–solid phase transition [1–6]. In this family $KMgF_3$ is a material of special interest because, up to now, no phase transition has been observed in this compound and hence it provides a good, stable matrix to be used to study the electronic properties of M^{2+} ions in a high-symmetry environment [7]. Moreover, a rigid-ion model (RIM) gives a reliable description of the dynamical properties of $KMgF_3$ because F^- and Mg^{2+} are small and weakly polarizable ions.

In this context, we have undertaken a study of the lattice vibrations of this perovskite-type crystal by inelastic neutron scattering in order to determine the parameters of a rigid-ion model defined by three pair interactions (K–F, Mg–F and F–F). Such a model allows us to calculate the phonon density of states which is of great interest for a quantitative interpretation of photon emission phemomena assisted by creation or annihilation of phonons. This work is also part of an extensive study of AMF_3 and MF_3 crystals [8] undertaken in order to define reliable interionic short-range potentials which can be easily transferred to other more complex structures [9] such as A_2MF_4 or ABF_4.

In this paper the experimental data are analysed in the framework of an RIM. In section 2 the inelastic neutron scattering measurements are described. In section 3, results of lattice dynamical calculations derived from the experimental phonon spectra are presented and compared with data obtained previously for other cubic fluoroperovskites.

2. Experimental details

Two series of inelastic neutron scattering measurements were performed at the Léon Brillouin Laboratory (LLB) on a large single crystal of $KMgF_3$ grown by the Czochralski technique [10, 11]. The volume of this sample is about 50 cm^3 and its mosaic spread less than 18′. All of the experiments were guided by detailed inelastic structure factor calculations based on RIMs incorporating the latest experimental results.

0953-8984/93/417615+08$07.50 © 1993 IOP Publishing Ltd

The first series of scans was carried out on the thermal beam triple-axis spectrometer 1T in phonon creation with a final wavevector fixed at $k_f = 2.662$ Å^{-1} ($\lambda = 2.36$ Å). The data of the second series were collected in phonon annihilation on the 4F1 triple-axis spectrometer installed on a cold source with an incident wavevector fixed at $k_i = 2.662$ Å^{-1}. In both cases, high-order contamination has been reduced with a pyrolytic graphite (PG 002) filter placed in the scattered and in the incident neutron beam respectively (the choice of a PG filter imposed the values of k_i and k_f).

In order to settle some questions left open by the first experiments, all the data collected on 4F1 were taken with horizontal collimations of 20′ (see table 1) to improve the resolution.

Table 1. Horizontal collimations used on the spectrometers 1T and 4F1, where S is the source, M the monochromator, Sa the sample, A the analyser and D the detector.

Spectrometer	S/M	M/Sa	Sa/A	A/D
1T	30′	40′	40′	40′
4F1	—	20′	20′	20′

All the measurements were performed at room temperature in three different scattering planes: $(hk0)$, (hhl) and $(3h, h, l)$ because some important modes are symmetry forbidden in the classical (hhl) diffusion plane.

3. Experimental results and lattice dynamical calculations

3.1. The lattice dynamical model

The measured phonon frequencies have been used to determine the force constants of an RIM. This quite simple model, which neglects polarizabilities, is especially suitable for the dynamical study of AMF_3 fluoroperovskites because most of the ions involved in these materials are weakly polarizable. As previously assumed by several authors [1, 12, 13], the model is defined by eight adjustable parameters: the ionic charges Z_K and Z_{Mg} (Z_F is given by the charge neutrality condition) and the longitudinal and transverse short-range force constants A_i and B_i, respectively, between neighbouring K–F, Mg–F and F–F ion pairs ($i = 1$–3 respectively).

In Cowley's notation these coefficients are given by the following expressions [13]:

$$A_i = (2v/e^2)(\partial^2 V_i/\partial r_{i\parallel}^2)_0 \qquad B_i = (2v/e^2)(\partial^2 V_i/\partial r_{i\perp}^2)_0$$

where v is the volume of the unit cell and V_i the interionic potential between the considered ions; the subscript 0 denotes the equilibrium position.

In the perovskite structure, since every ion is located at a centre of symmetry, the polarizabilities do not affect the elastic constants, which can be exactly expressed in terms of the eight former parameters. In the fitting procedure we followed Rousseau *et al* [1] and used the equations for the elastic constants as constraints. Thus we reduced the number of fitting parameters to five. As input constants we used the data of Rosenberg and Wigmore [14]

$$C_{11} = 132 \text{ GPa} \qquad C_{12} = 39.6 \text{ GPa} \qquad C_{44} = 48.5 \text{ GPa}.$$

It should be noted that the ratio $C_{12}/C_{44} = 0.82$ does not deviate very much from Cauchy's law [15], which indicates that the short-range pair potentials in $KMgF_3$ are not far from the spherical symmetry.

3.2. Experimental data

The phonon frequencies for wavevectors in the four main symmetry directions of the cubic Brillouin zone ΓR, ΓM, ΓX and RM (see figure 1) are shown in figure 2 together with the calculated dispersion curves obtained from the model RIMI, which will be discussed in detail below.

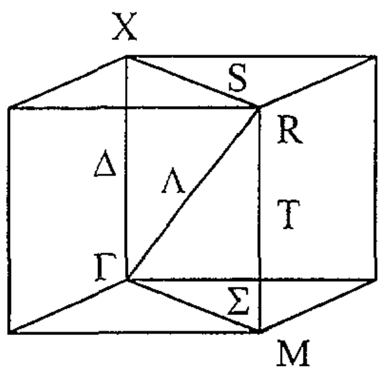

Figure 1. Representation of the high-symmetry points and lines of the cubic primitive Brillouin zone ($\frac{1}{8}$ of the zone).

Each measured phonon peak intensity I_{corr} is theoretically proportional to the square modulus of the dynamical structure factor of the q_j normal mode which is defined by

$$F_j(Q) = \sum_k \exp[-W_k(Q)] b_k^{coh} \exp(-i2\pi\boldsymbol{\tau}\cdot\boldsymbol{x}_k) \frac{\boldsymbol{Q}\cdot\boldsymbol{e}(k|\boldsymbol{q}_j)}{\sqrt{M_k}}$$

where the Debye–Waller factor $W_k(Q)$ is taken as a constant; $\boldsymbol{\tau}$ is a vector of the reciprocal lattice, $\boldsymbol{Q}$ is the momentum transfer ($\boldsymbol{Q} = 2\pi\boldsymbol{\tau} + \boldsymbol{q}$) and b_k^{coh} is the coherent scattering length of atom k of which the equilibrium position is defined by $\boldsymbol{x}_k$ in the original cell.

In preliminary measurements the R-point phonons R_{25} and R_{15}† (see figure 3) were determined in order to obtain a rough estimation of RIM parameters, which allowed us to calculate the dynamical structure factors (DSFs) at several points of the reciprocal lattice and, in this way, to prepare for the complete determination of the phonon dispersion curves.

In order to obtain the R_{15} and R_{25} normal mode frequencies, we chose the $\boldsymbol{Q}$ points of the reciprocal lattice where the DSFs of these modes were, because of their respective symmetry, different enough to discriminate between them. The R_{15} frequency was measured with a constant $\boldsymbol{Q}$ scan at $(\frac{3}{2}, \frac{3}{2}, \frac{3}{2})$ because the DSF of the R_{25} mode, whose eigenvectors involve rotations of octahedra around $\langle 100\rangle$ axes, is equal to zero for such $(\frac{1}{2}h, \frac{1}{2}h, \frac{1}{2}h)$ points of the reciprocal lattice. Thereafter the R_{25} normal-mode frequency was determined with an energy scan at $\boldsymbol{Q} = (\frac{3}{2}, \frac{3}{2}, \frac{5}{2})$ where the squared DSF of the R_{25} mode is about ten times larger than that of the R_{15} mode (see figure 3).

Thereafter, with the help of the inelastic structure factor calculations, we were able to assign almost every data point in the four main symmetry directions and to achieve the final refinements of the RIM.

It is worth noting that a comparison of the lowest phonon frequencies measured by inelastic neutron scattering at room temperature with the optically determined frequencies [16] shows an agreement to within 0.12 THz (i.e. 4 cm^{-1}) as shown in table 2.

† Throughout this paper, the irreducible representations will be labelled according to a choice of origin at a K site.

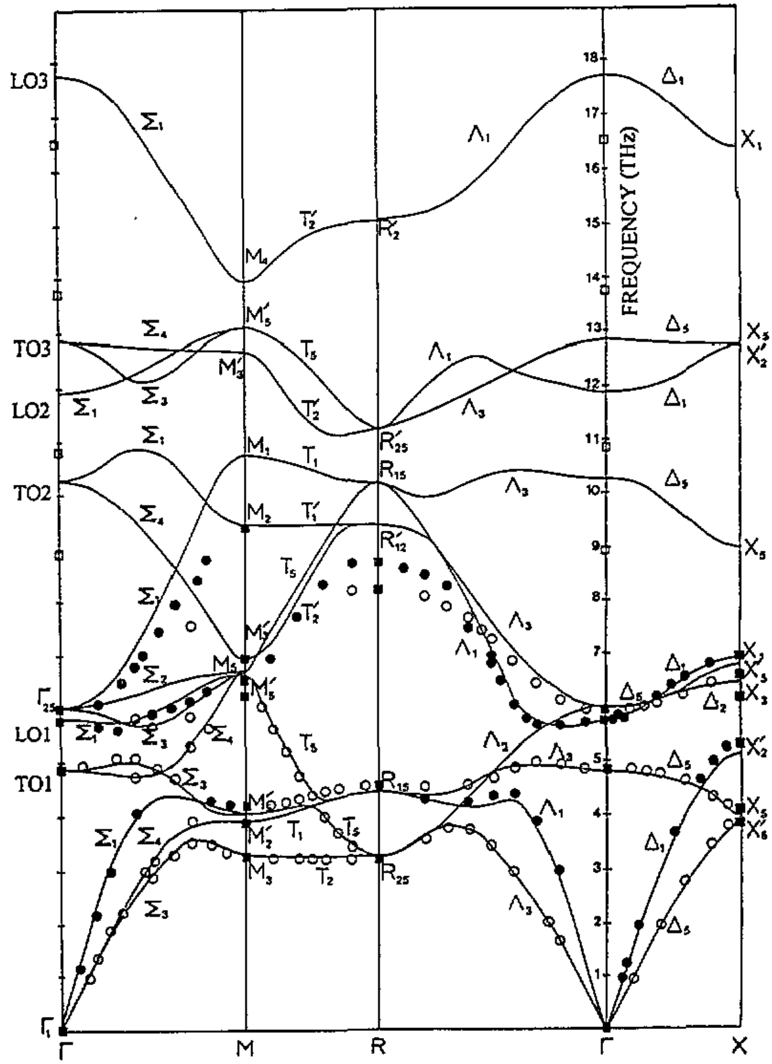

Figure 2. Phonon dispersion curves of $KMgF_3$ at room temperature. Circles are experimental frequencies of the phonons belonging to the different lines (open circles, transverse modes; filled circles, longitudinal modes). Filled squares represent measured phonons of the zone-boundary points; open squares are complementary infrared data taken from [16]. Full curves are theoretical dispersion curves calculated with RIM1.

3.3. Model calculations

Several different models lead to similar phonon dispersion curves. In order to make a choice based on physical assumption rather than on numerical values of refinement factor, we have selected two different models, RIM1 and RIM2 (see table 3) which fulfil the following conditions:

—all the B_i coefficients are negative, in agreement with a Born–Mayer modelling of the short-range interactions [1];

—the effective ionic charges are close to their free-ion values since the ionic

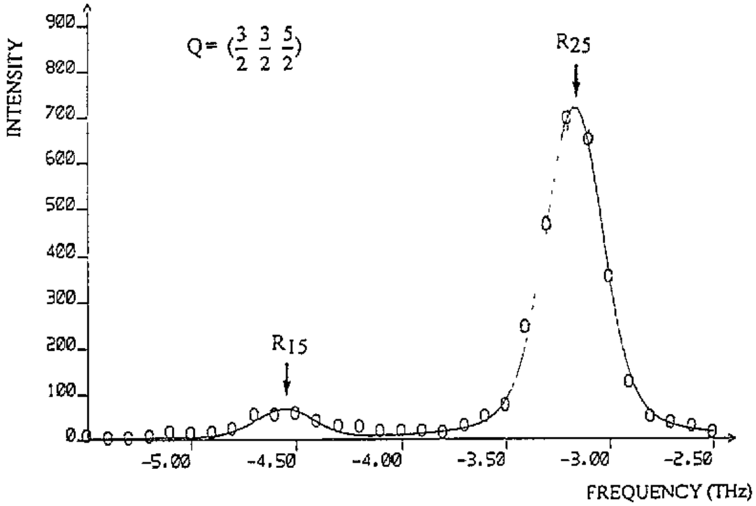

Figure 3. Inelastic neutron scattering scan used in the determination of the R$_{25}$ phonon frequency. The full curve represents the theoretical spectrum calculated with the fitting program of the LLB. Circles correspond to experimental points with error bars.

Table 2. Comparison at the centre of the Brillouin zone of phonon frequencies (given in cm^{-1}) measured by inelastic neutron scattering and infrared spectroscopy, with calculated frequencies (RIM1).

	Normal mode						
	TO1	LO1	Γ_{25}	TO2	LO2	TO3	LO3
ω (IR) [16]	168	197	silent	299	362	458	551
ω (Neutron)	164	195	198	—	—	—	—
ω (RIM1)	161	193	201	343	397	429	592

polarizabilities of the three types of ion involved in this compound (K^+, Mg^{2+} and F^-) are small.

Table 3. Parameters of the fitted rigid-ion models RIM1 and RIM2.

Model	A_1	B_1	A_2	B_2	A_3	B_3	Z_K	Z_{Mg}	Z_F
RIM1	7.66	−0.26	73.51	−9.6	4.29	−0.14	0.829	1.822	−0.883
RIM2	8.39	−0.42	81.37	−10.87	2.52	−0.13	0.915	1.929	−0.948

Although both models give phonon frequencies close to the experimental ones (see table 4), they differ significantly for the respective attribution of LO1 and Γ_{25} (triply degenerate) modes at the centre of the Brillouin zone on one hand, and X_5 and X'_5 zone boundary modes on the other hand (see table 5).

In this context, in order to discriminate between these two models, we have analysed carefully the scan profiles with a fitting program from the LLB [17] which takes into account both the shape of the dispersion curve (linear approximation) in the scattering plane, and the resolution function of each spectrometer including the mosaic spreads (monochromator,

Table 4. Comparison between experimental and calculated frequencies (in THz) of the normal modes at the high-symmetry points of the Brillouin zone.

	Normal mode								
	TO1	LO1	Γ_{25}	R_{25}	R_{15}	X_5'	X_5	M_3	M_2'
Experiment	4.91	5.83	5.94	3.18	4.55	3.86	4.13	3.20	3.93
RIM1	4.83	5.79	6.02	3.26	4.45	3.92	3.96	3.29	3.90
$\Delta\omega/\omega$ (%)	−1.4	−0.7	1.3	2.5	−2.2	1.5	−4.1	2.8	−0.7
RIM2	4.81	6.02	5.71	3.18	4.50	3.96	3.83	3.22	3.90
$\Delta\omega/\omega$ (%)	−2.0	3.20	−3.80	0	−1.10	2.60	−7.20	0.60	−0.70

Table 5. Experimental results used in the determination of the relative positions of normal modes at Γ and X points together with corresponding theoretical values of frequencies and squared dynamical structure factors F_1^2 and F_2^2 calculated within RIM1 and RIM2 respectively.

	ω (RIM1)	ω (RIM2)	ω (experimental)	Q_1	$F_1^2(Q_1)$	$F_2^2(Q_1)$	$I_{corr}(Q_1)$
Γ point	5.78 (LO1)	5.71 (Γ_{25})	5.83	(2,2,0)	1.10	0	5.25
	6.02 (Γ_{25})	6.02 (LO1)	5.91		0	1.13	0.01
X point	3.92 (X_5')	3.83 (X_5)	3.98	(2,2,1.5)	1.496	10.18	3.56
	3.95 (X_5)	3.96 (X_5')	4.08		12.98	1.592	28.62

	Q_2	$F_1^2(Q_2)$	$F_2^2(Q_2)$	$I_{corr}(Q_2)$
Γ point	(1,1,2)	0.025	2.53	0
		2.53	0.04	5.38
X point	(1,1,0.5)	0.375	0.792	7.24
		0.753	0.417	24.79

sample, analyser) and the divergences of the neutron beam. This operation yields the different phonon peak positions and their respective intensities and thus enabled us to choose the first model (RIM1) which gives a better description of both frequencies and structure factors of the normal modes.

It should be noted that, in most of the previous studies of lattice dynamics in the fluoroperovskites, the A_i/B_i ratios for the A–F and F–F interactions were taken to be equal to −10 and gave convenient results [1]. In this study, we could not impose these values because of the bad description of the phonon spectrum they gave. Thus we allowed these ratios to vary and the best results were obtained with $A_1/B_1 = A_3/B_3 = -30$ (RIM1).

3.4. Mean square displacements and phonon density of states

The mean square displacements (MSDs) are expressed in terms of eigenvalues $\omega^2(q, j)$ and eigenvector components $e_\alpha(k|q_j)$ of the dynamical matrix

$$B_{\alpha\beta}(k) = \langle u_\alpha(k)u_\beta(k)\rangle = \frac{\hbar}{2NM_k}\sum_{q_j}\frac{e_\alpha(k|q_j)e^*_\beta(k|q_j)}{\omega(q,j)}[2\bar{n}(q,j)+1]$$

where N is the number of q vectors involved in the summation and $\bar{n}(q, j)$ the Bose–Einstein occupancy factor of the normal mode considered.

This calculation yields values which may be compared to the experimental MSDs obtained for other fluoride perovskites. As shown in table 6, the MSDs in $KMgF_3$ are smaller than in any other fluoride perovskite presented there. In particular, $B_{22}(F_1)$ which characterizes the F^--ion mean square displacement perpendicular to the M–F–M bonds is much smaller than the corresponding value for $RbCaF_3$. This observation indicates that the lattice vibrations in $KMgF_3$ are much more harmonic than in most of the fluoroperovskites, which is in agreement with the stability of this compound, which does not undergo any phase transition.

In addition, the phonon density of states presented in figure 4 has been calculated within the model RIM1 as a function of phonon energy, solving the dynamical matrix in $10^6 q$ vectors forming a uniform mesh over the first Brillouin zone.

Table 6. Room-temperature MSDs given in Å^2 in AMF_3 perovskite-type compounds.

Compound	Reference	B(A)	B(M)	$B_{11}(F_1)$	$B_{22}(F_1)$
$KMgF_3$ (calculated)	This work	0.011	0.006	0.006	0.012
$KMgF_3$ (experimental)	[19]	—	—	0.002	0.012
$KZnF_3$	[20]	0.014	0.005	0.008	0.019
$RbCaF_3$	[21]	0.023	0.008	0.008	0.036
$RbCaF_3$	[19]	—	—	0.006	0.042

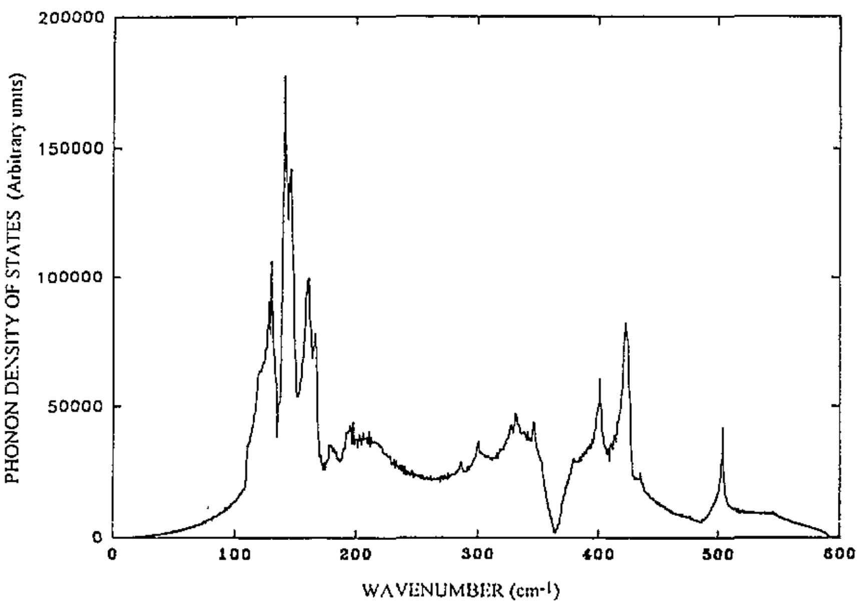

Figure 4. Histogram of the phonon density of states in $KMgF_3$ calculated with the rigid-ion model RIM1.

The first information given by this curve is that the Debye law ($g(\omega) = \alpha\omega^2$) is verified up to 55 cm^{-1}, which is the limit of the linear part of the acoustic branches. The next most important feature is the drastic enhancement of $g(\omega)$ at 108 cm^{-1} due to the flat T_2 branch.

A pseudo-gap is observed in the vicinity of 365 cm^{-1}. The cut-off frequency is close to 600 cm^{-1}, which is a higher value than generally observed in other fluoroperovskites (500 cm^{-1}). This can be attributed to strong coupling of light ions.

4. Conclusions

The lattice dynamics of the cubic fluoride perovskite $KMgF_3$ has been studied by means of inelastic neutron scattering measurements and analysed in terms of rigid-ion model parameters. The model calculations reproduce rather well the measured low- and medium-frequency phonons. Nevertheless, our fits are less satisfactory for high-energy branches and we will try, in a further study, to improve the model by introducing some other parameters such as those relating to the K–K interaction that have been neglected in spite of the relative proximity of these second-neighbour ions. The one-phonon density of states deduced from the present calculations is an important basis for the interpretation of the vibronic emission bands observed in $KMgF_3$ doped with transition ions such as Ni^{2+}, Mn^{2+} and Cr^{3+} in an Mg site [18].

A detailed comparative study of the short-range coefficients A_i and B_i deduced from the same model for other fluoroperovskites is in progress. We hope to extract from these results the parameters of a short-range Buckingham potential available for a wide range of F–F interatomic distances.

Acknowledgment

We are grateful to A Bulou for his participation in the neutron scattering experiments and for a critical reading of the manuscript.

References

[1] Rousseau M, Nouet J and Almairac R 1977 *J. Physique* **38** 1423–8
[2] Bulou A, Rousseau M and Nouet J 1992 *Diffusionless Phase Transitions and Related Structures in Oxides* Trans. Tech. ch 4, pp 133–86
[3] Gibaud A, Shapiro S M, Nouet J and You H 1991 *Phys. Rev.* B **44** 2437–43
[4] Toulouse J, Wang X Q and Rousseau M 1991 *Phys. Rev.* B **44** 6635–41
[5] Katrusiak A and Ratuszna A 1992 *Solid State Commun.* **84** 435–41
[6] Kassan-Ogly F A and Naish V E 1986 *Acta Crystallogr.* B **42** 297–306
[7] Russi R, Barbosa G A, Rousseau M and Gesland J Y 1984 *J. Physique* **45** 1773–8
[8] Daniel P, Bulou A, Rousseau M, Nouet J and Leblanc M 1990 *Phys. Rev.* B **42** 10545–52
[9] Bulou A, Rousseau M, Nouet J and Hennion B 1989 *J. Phys.: Condens. Matter* **1** 4553–83
[10] Gesland J Y 1980 *J. Cryst. Growth* **49** 771–4
[11] Baldochi S L and Gesland J Y 1992 *Mater. Res. Bull.* **27** 891–900
[12] Lehner N, Rauh H, Strobel K, Geick R, Heger G, Bouillot J, Renker B, Rousseau M and Stirling W G 1982 *J. Phys. C: Solid State Phys.* **15** 6545–64
[13] Cowley R A 1964 *Phys. Rev.* **134** 981–97
[14] Rosenberg H M and Wigmore J K 1967 *Phys. Lett.* **24A** 317
[15] Born M and Huang K 1954 *Dynamical Theory of Crystal Lattices* (Oxford: Oxford University Press)
[16] Perry C H and Young E F 1967 *J. Appl. Phys.* **38** 4616–24
[17] Hennion B private communication
[18] Mortier M *et al* to be published
[19] Jex H, Maetz J and Mullner M 1980 *Phys. Rev.* B **21** 1209–18
[20] Ridou C, Rousseau M, Pernot B and Bouillot J 1986 *J. Phys. C: Solid State Phys.* **19** 4847–53
[21] Bulou A, Ridou C, Rousseau M, Nouet J and Hewat A W 1980 *J. Physique* **41** 87–96